In Situ Electron Microscopy Four-Point Electromechanical Characterization of Freestanding Metallic and Semiconducting Nanowires

*Rodrigo A. Bernal, Tobin Filleter, Justin G. Connell, Kwonnam Sohn, Jiaxing Huang, Lincoln J. Lauhon, and Horacio D. Espinosa**

Electromechanical coupling is a topic of current interest in nanostructures, such as metallic and semiconducting nanowires, for a variety of electronic and energy applications. As a result, the determination of structure-property relations that dictate the electromechanical coupling requires the development of experimental tools to perform accurate metrology. Here, a novel micro-electro-mechanical system (MEMS) that allows integrated four-point, uniaxial, electromechanical measurements of freestanding nanostructures in-situ electron microscopy, is reported. Coupled mechanical and electrical measurements are carried out for penta-twinned silver nanowires, their resistance is identified as a function of strain, and it is shown that resistance variations are the result of nanowire dimensional changes. Furthermore, in situ SEM piezoresistive measurements on n-type, [111]-oriented silicon nanowires up to unprecedented levels of ~7% strain are demonstrated. The piezoresistance coefficients are found to be similar to bulk values. For both metallic and semiconducting nanowires, variations of the contact resistance as strain is applied are observed. These variations must be considered in the interpretation of future two-point electromechanical measurements.

1. Introduction

The coupling of mechanical and electrical properties in nanostructures has received increased attention given the major role they are envisioned to play in future electronic and electromechanical devices. For example, metallic nanowires can be used to probe the effects of scaling in the miniaturization of electronic interconnects,[1] or be used as interconnects themselves,[2] while semiconductor nanowires, with properties such as piezoresistivity[3] and piezoelectricity, find applications in sensors,[4] energy harvesting,[5] novel-architecture transistors[6] and nanoprocessors.[7]

In the context of metallic nanowires, the mechanical signature of electromigration and the electrical nature of dislocation activity remain to be studied. Electromigration is a likely failure mode in nano-sized interconnects as a result of higher current densities.[8] However, the stresses involved have not been deeply understood, although it was observed they are compressive.[9] Strengthening of metals using coherent twinning has resulted in a mild reduction in conductivity,[10] but its effect on electromigration remains unknown.[8] Since metallic nanowires with coherent twin boundaries have been synthesized,[11,12] they constitute an ideal test bed for studying electromigration in nano-sized interconnects and its

R. A. Bernal, T. Filleter,[+] Prof. H. D. Espinosa
Department of Mechanical Engineering
Northwestern University
Evanston, IL 60208, USA
E-mail: espinosa@northwestern.edu
J. G. Connell, Dr. K. Sohn,
Prof. J. Huang, Prof. L. J. Lauhon
Department of Materials Science and Engineering
Northwestern University
Evanston, IL 60208, USA
[+]Present address: Department of Mechanical and Industrial Engineering, University of Toronto, Toronto, ON M5S 3G8, Canada

DOI: 10.1002/smll.201300736

associated mechanical response.[8,9] On the other hand, dislocation activity has been correlated to the resistance-noise spectrum in macroscale metallic specimens,[13] but this phenomenon has not been yet studied in nanowires.

In semiconducting nanowires, increased attention has been paid to their electromechanical properties due to reports on giant piezoresistivity in silicon nanowires,[14] and energy harvesting using piezoelectric nanowires,[5] although some questions remain open.[15–17] Even though giant piezoresistance has been reported by several groups,[14,18,19] recent reports point to possible experimental artifacts that may explain earlier measurements.[15,16] In the case of energy harvesting, the correlation between conductivity, carrier concentration, and piezoelectric output has been the subject of controversy,[17,20,21] although such systems have demonstrated to produce usable electrical energy.[22] Computational studies have revealed giant piezoelectricity in gallium nitride (GaN) and zinc oxide (ZnO) nanowires of small diameters (<3nm),[23] and piezoelectric response for nanowires of non-piezoelectric materials,[24] but these phenomena remains to be experimentally demonstrated. Another material system of interest is vanadium dioxide nanowires, as phase transitions induced by temperature and strain have the potential to be used in electrical and optical switching.[25,26]

Due to this significant interest, development of novel experimental tools to accurately characterize electromechanical response in individual nanowires is needed, in order to achieve well defined and reproducible conditions leading to repeatable results. Even though individual-nanowire experiments are now possible, results are typically not consistent across the board, as alluded to above. To avoid ambiguities, complementary techniques such as individual-nanowire dopant characterization, and in-situ electron microscopy testing are preferred.[27] In-situ testing, in particular, allows high resolution and the capability to observe the sample and its structure as the experiment progresses.[28–30] In fact, in the context of mechanical testing, In situ Transmission Electron Microscopy (TEM) and Scanning Electron Microscopy (SEM) techniques do exist based on specialized TEM holders, Microelectromechanical Systems (MEMS), and resonance. (For detailed reviews see[28,31]).

In electromechanical studies of nanowires, the most common approach has been to deform the sample and measure the specimen's electrical response (resistivity, generated charge, etc.) using two electrical contacts (two-point measurement).[14] Although this may be appropriate for contacts that are co-synthesized with the sample,[14,32,33] it is well known that post-synthesis contacts add a contact resistance and may introduce Schottky barriers.

For the above reasons, four-point electrical measurements are preferred as they provide the true specimen resistance.[34] In fact, this method has been applied for several nanowire systems.[35–38] However, integration of four-point testing, mechanical deformation, and in situ electron microscopy observation in individual, freestanding nanowires has not been yet demonstrated. Ex situ designs have been proposed with MEMS technology, but they do not allow simultaneous electrical measurements and application of strain.[39,40] Similarly, although MEMS devices for nanowire testing with capabilities of sample straining and electrical measurements have been demonstrated,[41,42] they do not allow decoupling of the contact resistance. The examples highlight that integrating all these capabilities is not trivial due to the challenging nature of these experiments.

In this report, we demonstrate a MEMS device for four-point electromechanical characterization of freestanding nanowires in electron microscopes. In-situ SEM measurements were conducted on silver and silicon nanowires. For silver nanowires, we find a good match between experiments and theory in the elastic and plastic regimes, which validates the experimental method. In silicon nanowires, measurements of the piezoresistance were carried out up to levels of 7% strain. For both types of specimens, we also compare the apparent (two-point) and true (four-point) strain-induced changes in resistance. We conclude that contact resistance changes as strain is applied to the sample. This has major implications for future research in electromechanical measurements on nanostructures.

2. Device Description

The four-point MEMS device is built upon a proven system for mechanical characterization,[43–46] where a thermal actuator[44,45] is used to impose deformation on one end of the specimen. The other end of the specimen is connected to a capacitive load sensor.[43] This design has proved reliable in characterizing mechanical properties of nanowires,[47–50] carbon nanotubes,[51] and carbon nanotube bundles.[52]

Here, the fabrication process and design of the platform has been re-engineered to allow four independent electrical connections to the nanostructure. Specifically, as is shown in **Figure 1**a), four electrical *traces* coming from the outside electronics are connected by anchors and vias to very compliant, conductive *folded beams* that allow electrical access to the moving *shuttles* where the specimen is positioned. The folded beams are then interfaced with *interconnects* which are brought to the vicinities of the specimen (Figure 1b). The folded beams and interconnects are fabricated from highly-doped poly-silicon. In order to ensure that all four electrical signals are independent from each other, an insulating freestanding silicon nitride layer is deposited in the fabrication process.[29] In this way, mechanically connected structures are electrically insulated from each other. Specifically, the silicon nitride layer is used to fabricate two insulating *shuttles* where the specimen is positioned. At the same time, these shuttles provide mechanical connection to the thermal actuator and load sensor, and support for the poly-silicon interconnects.

To complete the electrical connections to the specimen, Ion or Electron-Beam-Induced platinum deposition (IBID or EBID) is used to pattern *connections* from the poly-silicon interconnects to the nanowire (Figure 1c). Two connections are performed on each end of the specimen. Under this configuration, four-point electrical measurements as a function of applied strain can be carried out. In particular, the true strain-induced variations in resistance of the freestanding portion of the specimen, between the two middle contacts, can be measured. The complete device is shown in Figure 1.

NANO MICRO small

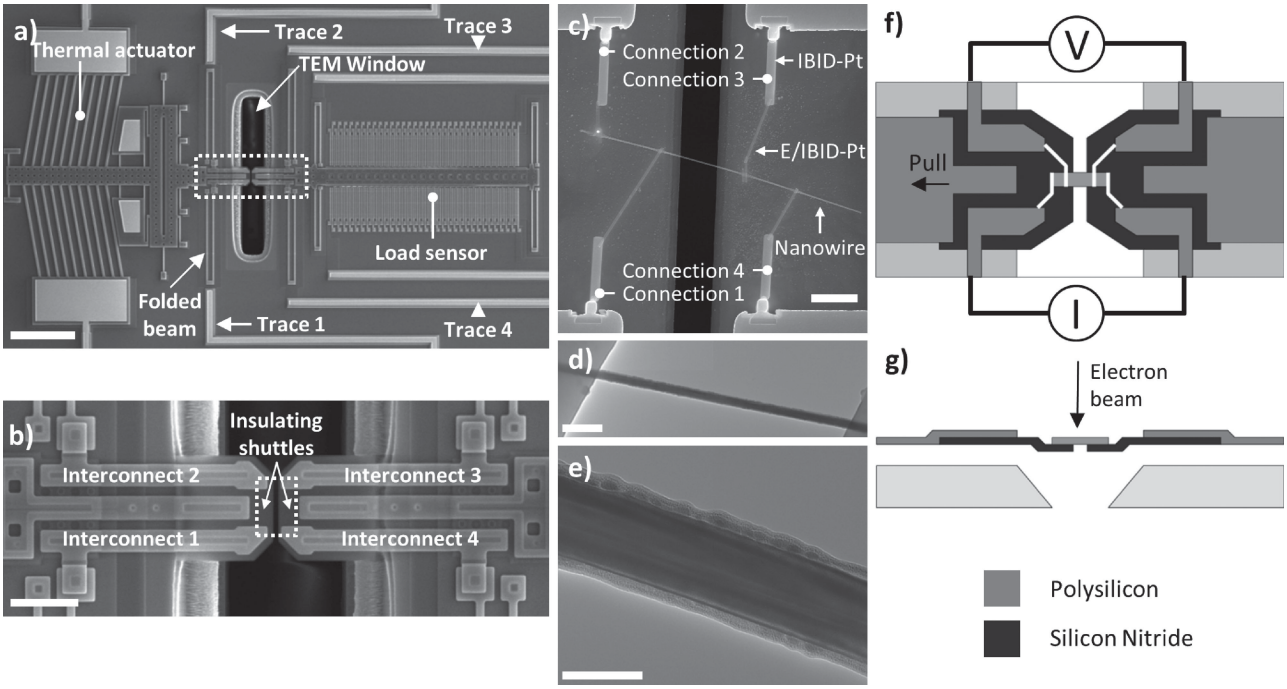

Figure 1. MEMS for four-point electromechanical measurements. a) SEM image showing an overview of the device. Scale bar: 200 µm. The dashed square is detailed in (b). Here, the folded beams (u-shaped) shown in (a) which provide electrical connections, extend on top of silicon nitride shuttles and come close to where the specimen is placed. The platforms ensure insulation among the four specimen connections and between other signals used to operate the device. Scale bar: 40 µm. A detail of the dashed square is provided in (c) where a nanowire laid on the insulating shuttle and connected in four-point configuration is shown. Scale bar: 4 µm. d,e) TEM images, as viewed through the TEM window, of the same nanowire in (c) are shown (300 nm and 100 nm scale bar, respectively). f) Top-view schematic of the device operation for four-point measurements. g) Cross-section of the device.

3. Results and Discussion

In situ SEM experiments were carried out in both metallic and semiconducting nanowires (see the Experimental Section for synthesis details). For the metallic case, we utilize penta-twined silver (Ag) nanowires, for which mechanical characterization was previously carried out utilizing similar MEMS-based methods.[50] These samples are ideal to validate the experimental technique since changes in the specimen resistance are expected to be dominated by dimensional variations, and thus a prediction of the electromechanical behavior can be confidently made and compared to the experimental results. We then utilize the system to carry out piezoresistive measurements in n-type, [111]-oriented, silicon nanowires, and to characterize the behavior of contact resistance in electromechanical experiments.

The nanowires were placed on the MEMS device in-situ SEM and electrically connected by FIB using IBID of platinum (see the Experimental Section).[36] Electrical leakage caused by possible diffusion of the Pt depositions is negligible (see Supporting Information). The MEMS device was then wire bonded and interfaced with the electronics (see the Experimental Section). For device actuation and nanowire-strain measurement, the protocols previously reported[44,46] were followed. In particular, the strain in the nanowire is obtained by measuring the displacement of the insulating shuttles from SEM images and dividing by the gage length. The calculation is corrected for misalignment between the nanowire and tensile axis as appropriate. Only nanowires with small misalignment were tested (worst case is 16°), resulting in a correction of less than 4%. This small misalignment, in combination with the large aspect ratio of the tested specimens, ensures that most of the gage section is in pure tension and that bending stresses near the boundaries are less than 10% of the axial stresses.[53] All electrical measurements were carried out with the electron beam turned off.

3.1. Specimen Resistance as a Function of Strain: Four-Point Measurements

3.1.1. Experiments in Silver Nanowires

Silver nanowires of different diameters (177 ± 2 nm, 65 ± 2 nm) were tested to validate the experimental method (**Figure 2**a,b). As expected, due to the relatively long electrical path and the use of platinum deposition, the measured two-point resistance is relatively high (Figure 2d). However, the measured four-point-resistance is much lower (Figure 2e). Using the four-point-resistance measurements at zero strain and SEM measurements of the nanowire diameter and length of the gage region, the resistivity of the samples is calculated to be $45 \pm 0.4 \times 10^{-9}$ Ωm and $87 \pm 4 \times 10^{-9}$ Ωm for the 177 and 65 nm nanowires, respectively. These values are in the same order of magnitude as the bulk resistivity of silver (16×10^{-9} Ωm).[54] A higher resistivity than bulk as

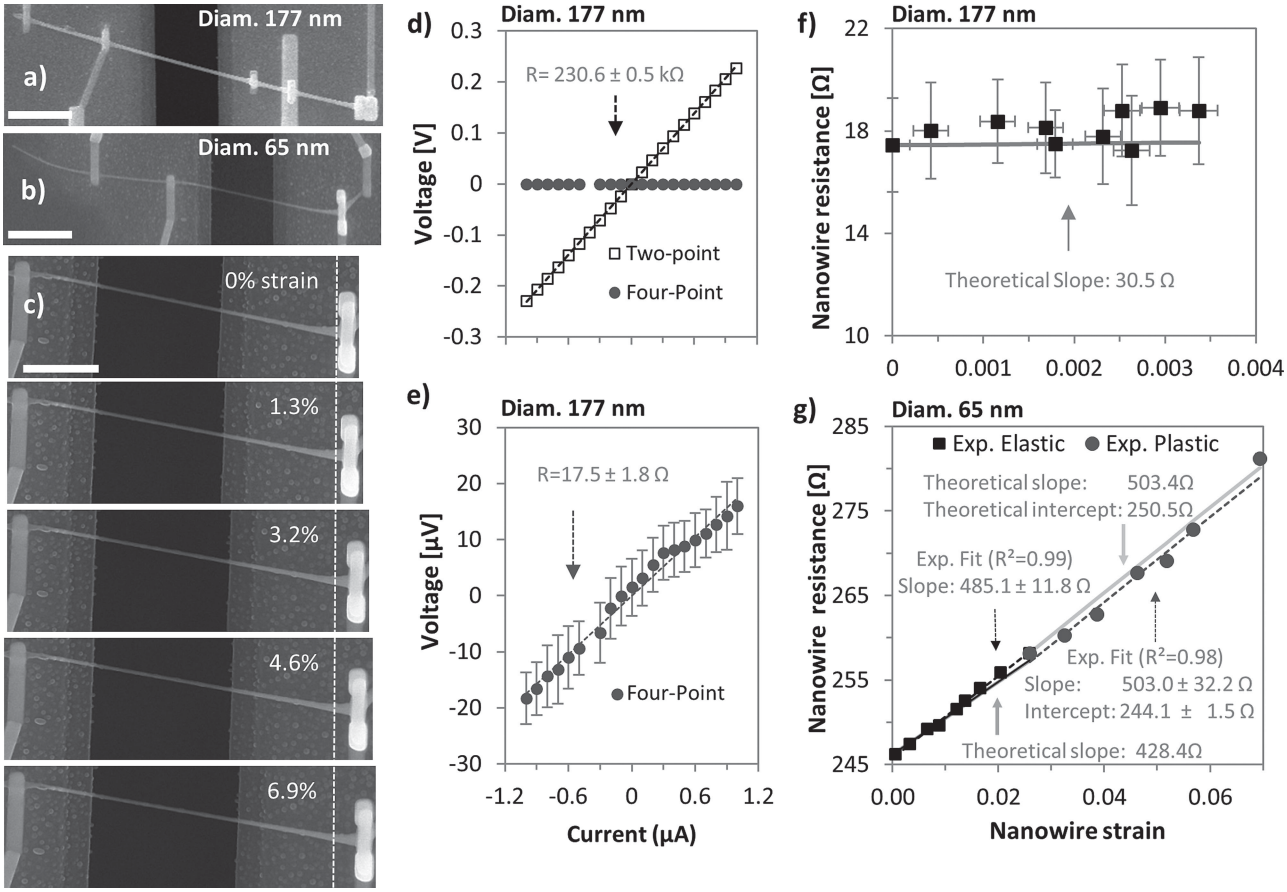

Figure 2. Electromechanical testing of silver nanowires. a–b) SEM Micrographs of the nanowires placed in the MEMS device for four-point testing. Scale bars are 3 μm. c) Sequential images of the 65 nm nanowire during electromechanical testing. Scale bar: 2 μm. d,e) Four-point and two-point current-voltage curves for the 177 nm nanowire at 0% strain. Figure e) shows the four-point curve in greater detail. f) 177 nm-nanowire resistance as a function of strain. No major changes are observed (see text). g) Resistance of the 65 nm nanowire as a function of strain.

specimen-dimension decreases can be expected given the increased surface scattering in the nanowire[54,55] and the influence of surface roughness.[35] Nanowires of gold with similar penta-twinned structure were demonstrated to have resistivity in the same order of magnitude of the bulk, and a similar behavior of increasing resistivity with decreasing diameter.[35]

The resistance of the nanowires was characterized as a function of strain. For low level of strains, the thick nanowire was employed, in order to test the resolution of the experimental method. The thin nanowire was stretched to higher strain (6.9%; Figure 2c) in order to probe the behavior of resistance in the plastic regime. The changes in specimen resistance with strain can be described, in the elastic regime as (see the Supporting Information for formal derivation):

$$R(\varepsilon) = R_0 \frac{(1+\varepsilon)}{(1-\nu_a \varepsilon)^2} \tag{1}$$

where R_0 is the resistance at zero strain, ε is the strain and ν_a is the averaged Poisson's ratio,[56] which is 0.37 for silver (See the Supporting Information). The averaged Poisson's ratio is used in order to take into account the changes in the cross-sectional area for an anisotropic specimen. Using a linear approximation around $\varepsilon = 0$, the resistance can be described as:

$$R \approx R_0 + \left[R_0(1+2\nu_a)\right]\varepsilon \tag{2}$$

As expected for the thick nanowire, the resistance as a function of strain shows little changes (see Figure 2f). In this case, variations of the resistance with the dimensional changes imposed in the sample are too small to be resolved. Given that the initial resistance and maximum strain were low, the change of resistance as a function of strain is expected to have a slope of 30.5 Ω, which is consistent with the measurements within experimental error as seen in Figure 2, although it is near the resolution limit of the technique.

For the thinner nanowire, tested at high strain (6.9 ± 0.1%), the changes of resistance in the elastic regime are more significant and follow closely the description of (2). In particular, the theoretically-predicted slope should have a value of 428.4 Ω which is very close to the experimentally-measured value of 485 ± 12 Ω, Figure 2g. The slight mismatch can be explained by the differences between the elastic constants of the nanowire and the bulk material. The elastic limit is taken as the closest lower experimental point with respect

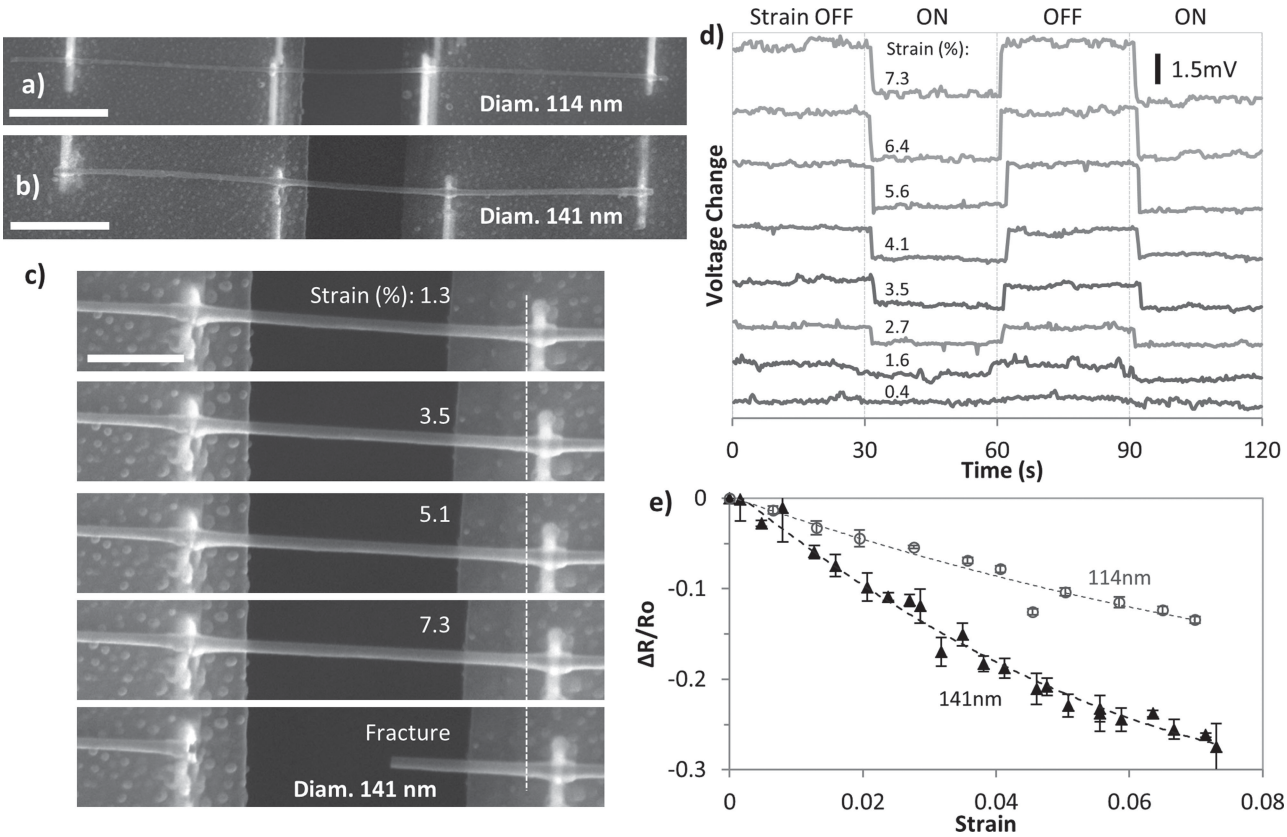

Figure 3. Electromechanical testing of Silicon nanowires. a,b) SEM Micrographs of the nanowires placed in the MEMS device for four-point testing (diameters 114 and 141 nm). Scale bar is 3 µm. c) Sequential images of the 141 nm nanowire during electromechanical testing and up to fracture above 7.3% strain d) Changes in voltage with a constant applied current, for different strain levels (141 nm nanowire). Note: the strain is modulated in order to directly correlate resistance change and applied strain (see text for details) e) Relative change of resistance for the two specimens as a function of strain. The dashed lines indicate a quadratic fit to the data.

to 3% strain (2.59 ± 0.08%). This transition point from elastic to plastic behavior is based on extensive and detailed in situ TEM stress-strain measurements and atomistic simulations, previously reported for the same penta-twinned Ag nanowires, which demonstrated their plastic deformation mechanisms, and revealed diameter independent yield strains of ~3%.[50]

The behavior of the specimen resistance in the plastic regime was also explored and is shown in Figure 2g. Here, the resistance change is expected to be governed by dimensional changes, which in plasticity can be computed using conservation of volume as follows:

$$R(\varepsilon) = R_y \frac{(1+\varepsilon)^2}{(1+\varepsilon_y)^2} \tag{3}$$

where R_y is the resistance at yielding (see the Supporting Information for formal derivation). To first order, this can be approximated around the yield point ε_y as:

$$R(\varepsilon) = R_y \frac{(1-\varepsilon_y)}{(1+\varepsilon_y)} + \left[2R_y \frac{1}{(1+\varepsilon_y)}\right]\varepsilon \tag{4}$$

Taking the yield point as the closest experimental point to 3%, $\varepsilon_y = 0.0259 \pm 0.0008$, and the resistance at yield $R_y = 258.2 \pm 0.1\Omega$ the calculated intercept (245.2 Ω) and slope (503.4 Ω) closely match a linear fit to the experimental data (244.1 ± 1.5 Ω, 503.0 ± 32.2 Ω).

Overall, these results validate the MEMS device as a tool to characterize the true strain-induced changes of resistance in one-dimensional nanostructures, by integrating four-point electrical measurements, sample straining, and in-situ electron microscopy testing.

3.1.2. Experiments in Silicon Nanowires

N-type silicon nanowires grown along the [111] axis with different diameters (141 ± 6, 114 ± 4 nm) were tested as well. The specimens are shown in **Figure 3**, along with the associated measurements. The nanowires were tensioned up to fracture, therefore allowing piezoresistive measurements at high levels of strain (7.0% and 7.3% strain respectively; see Figure 3c). Fracture strains of this magnitude are typical for semiconducting nanowires due to lower defect densities as material dimensions are reduced.[47,57] In order to measure the change in resistance with applied strain, the strain-modulation technique[16] was employed (Figure 3d). Strain was applied and removed ("ON-OFF") alternately while applying a constant current (50 nA) and measuring the change in voltage. Thus, this technique produces a change in resistance that is directly correlated to strain, unaffected by longer time-scale resistivity drift due to other causes, such as charge trapping.[16]

For both nanowires, we observe a reduction of resistance as strain is applied. This is consistent with the piezoresistance behavior of [111], n-type bulk silicon.[58] Although both nanowires show similar changes for small strains (<1%), their behaviors diverge for larger values. A slight deviation from linear behavior is seen above ~4% strain. In contrast to the results in p-type Si nanowires by Lugstein et al.,[37] we do not observe an inversion of the sign of the piezoresistance at high strains. Note however, that the nanowires are expected to have a high carrier concentration[59] (see the Experimental Section), and display ohmic behavior, as opposed to space-charge-limited transport.

The relative change in resistance in the nanowires can be expressed as[58]:

$$\frac{\Delta R}{R_0}(\varepsilon) = (1 + 2\nu)\varepsilon + \frac{\Delta\rho}{\rho_0} \quad (5)$$

where ν is the Poisson's ratio (0.18 for silicon – uniaxial strain in the [111] direction[60]) and ρ is the resistivity. The relative change in resistivity, excluding dimensional changes, that is, the piezoresistance, can be thus obtained from the experimental data and fit to a polynomial to extract the longitudinal piezoresistance coefficients. A better fit is found with a second order ($R^2 = 0.99$–0.98), rather than with a linear polynomial ($R^2 = 0.97$), due to the slight nonlinearity observed in the data. The corresponding piezoresistance coefficients are $\pi_1^{[111]} = -3.7 \times 10^{-11}$ Pa^{-1}, $\pi_2^{[111]} = 6.9 \times 10^{-22}$ Pa^{-2} for the 141 nm nanowire, and $\pi_1^{[111]} = -2.1 \times 10^{-11}$ Pa^{-1}, $\pi_2^{[111]}$ 2.2×10^{-22} Pa^{-2} for the 114 nm nanowire. The first order coefficients are comparable to the coefficients for n-type bulk silicon in the [111] direction (-7.53×10^{-11} Pa)[58] and are consistent with recent experimental findings that indicate that silicon nanowire piezoresistance, although possibly dependent on size, is generally of the same order of magnitude as bulk.[16,61]

However, the difference in the piezoresistance coefficients for the two tested nanowires cannot be solely attributed to a size-effect, given that exact doping levels of the individual nanowires are not known. Even when doping levels are similar, the absolute concentration of dopants differs from the concentration of active dopants.[59] As it has been pointed out recently,[27] complementary methods for dopant characterization in individual nanowires, such as atom probe tomography,[62,63] and measurements of carrier mobility and concentration through recently-developed individual-nanowire Hall measurements,[64] are necessary to achieve a more complete picture of electromechanical behavior.

3.2. Behavior of the Contact Resistance with Strain

The two-point nanowire resistance, measured between the two innermost terminals contacting the sample, was also recorded as a function of strain for both metallic and semiconducting nanowires (see the Experimental Section). This resistance has contributions from the nanowire, the IBID and polysilicon interconnects, and the contact resistance between the nanowire and the IBID. For metallic nanowires, the nanowire and IBID resistances are negligible compared to the two-point resistance, and therefore the two-point measurement represents the contact resistance. For silicon nanowires, this assumption is no longer true, but we can compare the relative change in two-point resistance ($\Delta R^{2\text{-point}}/R_0^{2\text{-point}}$) with the values obtained from the four-point measurements, as shown in **Figure 4**.

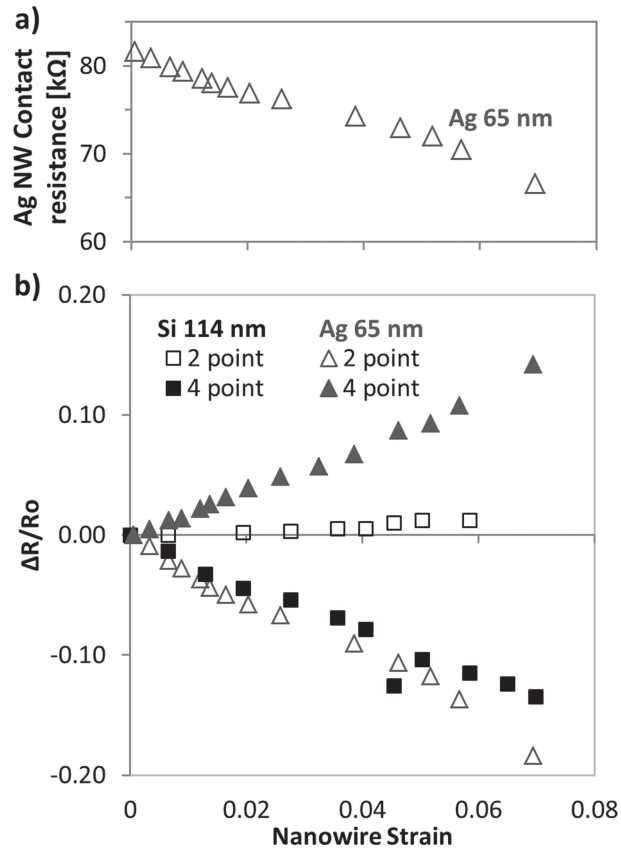

Figure 4. Comparison of two-point and four-point electromechanical measurements in silver and silicon nanowires. a) Behavior of the contact resistance in the 65 nm silver nanowire as a function of strain. b) Comparison of the relative change of resistance obtained using two and four-point measurements for the 65 nm silver, and 114 nm silicon nanowires.

The contact resistance to metallic nanowires decreases as strain is applied to the specimen (Figure 4a), whereas the actual nanowire resistance increases (Figure 4b). In both metallic and semiconducting nanowires, the relative change of resistance obtained from two-point measurements is different from the true relative change of resistance in the nanowire, obtained from four-point measurements. It is possible that the contact resistance is affected by local amorphization of the nanowire, which could have occurred in the area where the FIB contact was deposited. FIB-induced amorphization has been shown to decrease the contact resistance in GaN nanowires[65] although for the current results it does not explain why there is a change in contact resistance correlated to strain as well. On the other hand, increasing shear stresses develop in response to increasing nanowire strain at the nanowire/contact interface. This phenomenon may play a role in the reduction of the contact resistance as well. Although the exact mechanism governing the change in

contact resistance is unknown at this point, the results suggest the possibility of a strain-dependent contact resistance, which must be considered for the accurate interpretation of two-point electromechanical measurements.

4. Conclusion

In summary, a novel microsystem for in-situ four-point electromechanical measurements of freestanding nanowires was designed and demonstrated. The technique was validated by carrying out in-situ electron-microscopy tests of penta-twinned silver nanowires. Measurements of the zero-strain resistivity were found to be of the same order of magnitude as the bulk value, and larger for thinner nanowires in agreement with prior experimental results.[35] Changes in resistance with applied strain were found to be consistent with dimensional changes predicted by elasticity and plasticity theory.

The piezoresistance of [111] n-type silicon nanowires was measured up to 7% strain, a level that is, to our knowledge, unprecedented in the literature. The first order piezoresistive coefficients were found to be of similar magnitude as the bulk value, in agreement with recent experimental findings.[16, 61] Further studies are necessary to understand if the decrease of the piezoresistance coefficient with size is a result of a size effect, or a variation of the carrier concentration is also influencing the behavior.

Furthermore, it was demonstrated that the two-point measurement of nanowire resistance with applied strain is influenced by variations in the contact resistance, and *did not represent the true changes in the specimen resistance*. Although the changes in contact resistance in an electromechanical test may be particular to each individual setup, the experimental method presented here shares some features with other methods, namely, the use of post- growth metallization (EBID or IBID) to establish electrical and/or mechanical connections. If the variations in contact resistance are associated with FIB or electron-beam deposited metals, alternative methods of contacting *freestanding* nanostructures should be developed. On the other hand, if the variations are a result of mechanical stresses, they will play a significant role in future electromechanical characterization and will have to be considered regardless of the contacting technique. Note that not all electromechanical measurements may be amenable for implementation in a four-point configuration, for example, the measurement of charge in a piezoelectric experiment. However, our results suggest that for those cases one should characterize the behavior of the contact resistance with applied force or strain, or design experiments where contact resistance does not play a role.

Finally, we have provided basic design elements for the implementation of four-point electromechanical characterization of freestanding nanostructures, namely, i) a specimen placed between two movable, insulating platforms or shuttles and ii) the patterning of two contacts at each end, which can be incorporated into other microsystem designs. The capability of the system of allowing TEM observation should enable probing the structural features of electromechanical behavior in nanostructures in the near future. The implementation of in-situ electron microscope, four-point electromechanical testing, should lead to further understanding of the electromechanical coupling in nanostructures and associated size effects.

5. Experimental Section

Sample Preparation: The metallic nanowires tested are FCC silver (Ag) with a penta-twinned structure. The nanowires contain five single crystals, where the [110] axis is parallel to the long axis of the nanowire. The five crystals are separated by a twin boundary in the [111] plane.[66] The nanowires were prepared by a chemical method in which silver particles in a precursor solution are employed as seeds for nanowire growth. The one-dimensional growth is stabilized by a polymer (polyvinylpyrrolidone- PVP) which passivates the growth in the radial direction.[11] The process yields a liquid suspension of nanowires with typical lengths in the range of 5–20 μm.[67]

The silicon nanowires were grown using a hot-wall low-pressure chemical vapor deposition (LPCVD) reactor. Growth was performed for 15 minutes at a temperature of 460 °C and a total reactor pressure of 40 Torr, using 100 and 150 nm Au nanoparticles as catalysts. High-purity SiH_4 served as the semiconductor precursor gas, PH_3 (200 ppm in He) served as the *n*-doping precursor gas, and He served as the carrier gas with flows of 2, 20 and 30 standard cubic centimeters per minute (sccm), respectively. After growth, a small piece of the substrate was sonicated in isopropyl alcohol, yielding nanowires in liquid suspension.

Subsequently, the nanowire solutions were drop-casted onto TEM grids. Suitable nanowires for testing were selected and transported to the device in-situ SEM using a tungsten probe connected to a Klocke piezoelectric nanomanipulator. The device was then transported to a dual beam SEM/FIB system to perform the electrical connections.

In the FIB system, IBID of platinum was performed with 30 kV beam energy and 9.7–28pA current to create connections from the highly doped poly-silicon interconnects to the nanowires.[36] Care was taken in order to never expose the gage region of the nanowire to the ion-beam and to expose minimally the region between the current and voltage terminals in either side of the gage length.

Electrical Setup and Four Point Testing: A Keithley 4200 Semiconductor Characterization System (SCS) (current resolution 50 pA, voltage resolution 50 μV) was used to impose specific currents to the outer terminals of the sample. The induced voltage on the two inner terminals was measured using an Agilent 34401A Multimeter (0.1 μV voltage resolution) with a high (>10 GΩ) input resistance. All cable shields were tied to the electron microscope chamber, providing full shielding to the experimental setup.

The four point resistance was computed as the voltage measured by the multimeter, divided by the current applied by the Keithley SCS. For metallic nanowires, it was obtained by sweeping current through the sample (–1 μA to 1 μA in 100 nA steps, step duration ~30 s) and capturing the voltage value for each step of current, for each level of strain. The voltages reported are an average of the voltage measured during 30 s of each particular current step. The resistance is taken as the slope of the I–V curve to correct for any influence of thermal offset voltages, which may

be significant for these low-resistance samples.[68] For silicon nanowires, a current of 50nA is applied while the strain is alternated between zero and the value of interest several times with an interval of 30 s. The recorded differences of voltage are averaged and used to calculate an average change in resistance. For measurements of the two-point resistance, the Keithley SCS was connected to the inner terminals and the procedures for application of strain, previously followed for the four-point measurements, were repeated, all while measuring current and voltage.

Supporting Information

Supporting Information is available from the Wiley Online Library or from the author.

Acknowledgments

H. D. E. acknowledges support from NSF through award No. DMR-0907196. J.H. acknowledges support from Northwestern University Materials Research Science & Engineering Center (NU-MRSEC, NSF DMR-0520513). K.K. acknowledges partial support from the Leading Foreign Research Institute Recruitment Program through the National Research Foundation of Korea funded by the Ministry of Education, Science and Technology (2011–0030065). L.J.L acknowledges support from NSF through award No. DMR-1006069. We thank Benjamin Myers for useful discussions regarding FIB techniques. Part of this work was performed in the EPIC facility of NUANCE Center at Northwestern University. NUANCE Center is supported by NSF-NSEC, NSF-MRSEC, Keck Foundation, the State of Illinois, and Northwestern University.

[1] X. Liu, J. Zhu, C. Jin, L.-M. Peng, D. Tang, H. Cheng, *Nanotechnology* **2008**, *19*(8), 085711.
[2] Y. Wu, J. Xiang, C. Yang, W. Lu, C. M. Lieber, *Nature* **2004**, *430*(6995), 61–65.
[3] A. A. Barlian, W. T. Park, J. R. Mallon, A. J. Rastegar, B. L. Pruitt, *Proc. IEEE* **2009**, *97*(3), 513–552.
[4] J. Zhou, Y. Gu, P. Fei, W. Mai, Y. Gao, R. Yang, G. Bao, Z. L. Wang, *Nano Lett.* **2008**, *8*(9), 3035–3040.
[5] Z. L. Wang, J. Song, *Science* **2006**, *312*, 242.
[6] J. Raskin, J. Colinge, I. Ferain, A. Kranti, C. Lee, N. D. Akhavan, R. Yan, P. Razavi, R. Yu, *Appl. Phys. Lett.* **2010**, *97*(4), 042114.
[7] H. Yan, H. S. Choe, S. W. Nam, Y. J. Hu, S. Das, J. F. Klemic, J. C. Ellenbogen, C. M. Lieber, *Nature* **2011**, *470*(7333), 240–244.
[8] K. Lu, L. Lu, S. Suresh, *Science* **2009**, *324*(5925), 349–352.
[9] S. Fujisawa, T. Kikkawa, T. Kizuka, *Japn. J. Appl. Phys.* **2003**, *42*, L1433.
[10] L. Lu, Y. Shen, X. Chen, L. Qian, K. Lu, *Science* **2004**, *304*(5669), 422–426.
[11] B. Wiley, Y. Sun, Y. Xia, *Acc. Chem. Res.* **2007**, *40*(10), 1067–1076.
[12] F. Kim, K. Sohn, J. S. Wu, J. X. Huang, *J. Am. Chem. Soc.* **2008**, *130*(44), 14442–+.
[13] N. Bellido, A. Pautrat, C. Keller, E. Hug, *Phys. Rev. B* **2011**, *83*(10).
[14] R. R. He, P. Yang, *Nat. Nanotechnol.* **2006**, *1*, 42–46.
[15] A. C. H. Rowe, *Nat. Nanotechnol.* **2008**, *3*(6), 311–312.
[16] J. S. Milne, A. C. H. Rowe, S. Arscott, C. Renner, *Phys. Rev. Lett.* **2010**, *105*(22), 226802.
[17] M. Alexe, S. Senz, M. A. Schubert, D. Hesse, U. G. Sele, *Adv. Mater.* **2008**, *20*(24), 4021–4026.
[18] T. Barwicz, *Appl. Phys. Lett.* **2010**, *97*(2), 023110.
[19] P. Neuzil, C. C. Wong, J. Reboud, *Nano Lett.* **2010**, *10*(4), 1248–1252.
[20] Z. L. Wang, *Adv. Mat.* **2009**, *21*(13), 1311–1315.
[21] Y. Gao, Z. L. Wang, *Nano Lett.* **2009**, *9*(3), 1103–1110.
[22] Y. Hu, Y. Zhang, C. Xu, G. Zhu, Z. L. Wang, *Nano Lett.* **2010**, *10*(12), 5025–5031.
[23] R. Agrawal, H. D. Espinosa, *Nano Lett.* **2011**, *11*(2), 786–790.
[24] S. X. Dai, M. Gharbi, P. Sharma, H. S. Park, *J. Appl. Phys.* **2011**, *110*(10).
[25] J. Wei, Z. H. Wang, W. Chen, D. H. Cobden, *Nat. Nano.* **2009**, *4*(7), 420–424.
[26] H. Guo, K. Chen, Y. Oh, K. Wang, C. Dejoie, S. A. S. Asif, O. L. Warren, Z. W. Shan, J. Wu, A. M. Minor, *Nano Lett.* **2011**, *11*(8), 3207–3213.
[27] H. D. Espinosa, R. A. Bernal, M. Minary-Jolandan, *Adv. Mater.* **2012**, *24*(34), 4656–4675.
[28] R. Agrawal, H. D. Espinosa, *J. Eng. Mater. T- ASME* **2009**, *131*(4), 0412081–04120815.
[29] M. A. Haque, H. D. Espinosa, H. J. Lee, *MRS Bull.* **2010**, *35*, 375.
[30] M. Legros, D. S. Gianola, C. Motz, *MRS Bull.* **2010**, *35*, 354–360.
[31] H. D. Espinosa, R. A. Bernal, T. Filleter, *Small* **2012**, *8*(21), 3233–3252.
[32] H. Ohnishi, Y. Kondo, K. Takayanagi, *Nature* **1998**, *395*(6704), 780–783.
[33] K. H. Liu, W. L. Wang, Z. Xu, L. Liao, X. D. Bai, E. G. Wang, *Appl. Phys. Lett.* **2006**, *89*(22), 221908–3.
[34] P. Blood, J. W. Orton, *The electrical characterization of semiconductors : majority carriers and electron states* Academic Press London **1992**.
[35] K. Critchley, B. P. Khanal, M. Ł. Górzny, L. Vigderman, S. D. Evans, E. R. Zubarev, N. A. Kotov, *Adv. Mat.* **2010**, *22*(21), 2338–2342.
[36] A. Motayed, A. V. Davydov, M. D. Vaudin, I. Levin, J. Melngailis, S. N. Mohammad, *J. Appl. Phys.* **2006**, *100*(2), 024306–8.
[37] A. Lugstein, M. Steinmair, A. Steiger, H. Kosina, E. Bertagnolli, *Nano Lett.* **2010**, *10*(8), 3204–3208.
[38] S. E. Mohney, Y. Wang, M. A. Cabassi, K. K. Lew, S. Dey, J. M. Redwing, T. S. Mayer, *Solid-State Electron.* **2005**, *49*(2), 227–232.
[39] S. Y. Xu, J. Xu, M. L. Tian, *Nanotechnology* **2006**, *17*(5), 1470.
[40] J. H. Han, M. T. A. Saif, *Rev. Sci. Inst.* **2006**, *77*(4), 045102–8.
[41] D. Zhang, W. Drissen, J.-M. Breguet, R. Clavel, J. Michler, *J. Micromech. Microeng.* **2009**, *19*(7), 075003.
[42] Y. Zhang, X. Liu, C. Ru, Y. L. Zhang, L. Dong, Y. Sun, *J. Microelectromech. Syst.* **2011**, *PP*(99), 1–9.
[43] Y. Zhu, N. Moldovan, H. D. Espinosa, *Appl. Phys. Lett.* **2005**, *86*(1), 013506.
[44] Y. Zhu, H. D. Espinosa, *Proc. Natl. Acad. Sci. USA* **2005**, *102*(41), 14503–14508.
[45] Y. Zhu, A. Corigliano, H. D. Espinosa, *J. Micromech. Microeng.* **2006**, *16*(2), 242–253.
[46] H. D. Espinosa, Y. Zhu, N. Moldovan, *JMEMS* **2007**, *16*(5), 1219–1231.
[47] R. Agrawal, B. Peng, H. D. Espinosa, *Nano Lett.* **2009**, *9*(12), 4177–4183.
[48] R. Agrawal, B. Peng, E. E. Gdoutos, H. D. Espinosa, *Nano Lett.* **2008**, *8*(11), 3668–3674.
[49] R. A. Bernal, R. Agrawal, B. Peng, K. A. Bertness, N. A. Sanford, A. V. Davydov, H. D. Espinosa, *Nano Lett.* **2010**, *11*(2), 548–555.
[50] T. Filleter, S. Ryu, K. Kang, J. Yin, R. Bernal, K. Sohn, S. Li, J. Huang, W. Cai, H. D. Espinosa, *Small* **2012**, *8*(19), 2986–2993.

[51] B. Peng, M. Locascio, P. Zapol, S. Li, S. L. Mielke, G. C. Schatz, H. D. Espinosa, *Nat. Nano.* **2008**, *3*(10), 626–631.
[52] T. Filleter, R. Bernal, S. Li, H. D. Espinosa, *Adv. Mat.* **2011**, *23*, 2855–2860.
[53] W. Kang, M. T. A. Saif, *JMEMS* **2010**, *19*(6), 1309–1321.
[54] B. J. Wiley, Z. Wang, J. Wei, Y. Yin, D. H. Cobden, Y. Xia, *Nano Lett.* **2006**, *6*(10), 2273–2278.
[55] C. Durkan, *Current at the Nanoscale: An Introduction to Nanoelectronics,* Imperial College Press, London **2002**.
[56] S. P. Tokmakova, *Phys. Stat. Solidi B* **2005**, *242*(3), 721–729.
[57] Y. Zhu, F. Xu, Q. Q. Qin, W. Y. Fung, W. Lu, *Nano Lett.* **2009**, *9*(11), 3934–3939.
[58] Y. Kanda, *Sens. Actuators, A* **1991**, *28*(2), 83–91.
[59] E. Koren, J. K. Hyun, U. Givan, E. R. Hemesath, L. J. Lauhon, Y. Rosenwaks, *Nano Lett.* **2011**, *11*(1), 183–187.
[60] J. J. Wortman, R. A. Evans, *J. Appl. Phys.* **1965**, *36*(1), 153–156.
[61] A. Koumela, D. Mercier, C. Dupre, G. Jourdan, C. Marcoux, E. Ollier, S. T. Purcell, L. Duraffourg, *Nanotechnology* **2011**, *22*(39).
[62] J. G. Connell, K. Yoon, D. E. Perea, E. J. Schwalbach, P. W. Voorhees, L. J. Lauhon, *Nano Lett.* **2013**, *13*(1), 199–206.
[63] D. E. Perea, E. R. Hemesath, E. J. Schwalbach, J. L. Lensch-Falk, P. W. Voorhees, L. J. Lauhon, *Nat. Nanotechnol.* **2009**, *4*(5), 315–319.
[64] K. Storm, F. Halvardsson, M. Heurlin, D. Lindgren, A. Gustafsson, P. M. Wu, B. Monemar, L. Samuelson, *Nat. Nanotechnol.* **2012**, *7*(11), 718–722.
[65] C. Y. Nam, D. Tham, J. E. Fischer, *Nano Lett.* **2005**, *5*(10), 2029–2033.
[66] C. J. Johnson, E. Dujardin, S. A. Davis, C. J. Murphy, S. Mann, *J. Mater. Chem.* **2002**, *12*(6), 1765–1770.
[67] K. C. Pradel, K. Sohn, J. X. Huang, *Angew. Chem. Int. Ed.* **2011**, *50*(15), 3412–3416.
[68] *Low Level Measurements Handbook: Precision DC Current, Voltage, and Resistance Measurements*, Sixth ed, Keithley Instruments Inc, Cleveland **2004**.

Received: March 7, 2013
Published online: September 24, 2013